

## Observation of Growth Steps, Spiral Dislocations and Molecular Packing on the Surface of Lysozyme Crystals with the Atomic Force Microscope

BY JOHN H. KONNERT, PETER D'ANTONIO AND KEITH B. WARD

Laboratory for the Structure of Matter, Naval Research Laboratory, Washington, DC 20375, USA

(Received 21 October 1993; accepted 14 February 1994)

### Abstract

The (110) faces of lysozyme crystals in their mother liquor have been investigated using an atomic force microscope (AFM) in height mode. Crystal growth and dissolution steps, as well as simultaneous growth and dissolution in pits, have been observed. Screw dislocations were also observed but the fine structure has not yet been investigated. Images that may possess molecular resolution were obtained and compared with theoretical images based on the crystallographic structure and the effects of arbitrary tip profiles. Crystallographic periodicities of 38 and 112 Å were observed. A recurring feature is a centered periodic array of minima that may be associated with one of the two nearly planar sheets of molecules present in the crystal that are parallel to the (110) faces.

### 1. Introduction

Durbin & Carlson (1992) demonstrated that the atomic force microscope (AFM) could be used to observe growth steps on the surfaces of lysozyme crystals in their mother liquor. They observed the time course of nucleation, spreading and merging of two-dimensional islands to form successive layers of the crystal. More recently, Durbin (1993) has reported the observation of screw dislocations.

We have undertaken this study to complement the work of Durbin *et al.* by exploring the capabilities of an alternative image-collection technique. A brief description of the microscope will provide the basis for understanding the two primary methods of data collection. Our AFM, a Digital Instruments (1990) Nanaoscope II, utilizes piezoelectric crystals to scan the sample under a tip that is maintained in contact with the surface. The tip contacting the surface is attached to a cantilever (see Fig. 1), the deflection of which is monitored with a reflected laser beam. The deflections of the beam are measured with a two-component diode. The difference signal ( $A - B$ ) between the two diode components controls a feedback loop that translates the sample in the  $z$  direc-

tion in order that a nearly constant cantilever deflection be maintained. This results in a nearly constant force being applied to the sample surface.

AFM data may be collected by operating the microscope in either force mode or height mode. In height mode, the translation of the  $Z$  piezoelectric crystal is recorded *versus* the  $x$  and  $y$  positions of the tip. In this way a three-dimensional record of the surface is obtained. In force mode, the diode signal, ( $A - B$ ), indicating tip deflection is recorded *versus* the positions of the tip. Although the force mode does not yield three-dimensional data, it produces a very clear picture of abrupt changes in surface topology. Thus, this mode is ideal for observing where growth steps occur on the surface of protein crystals. These steps are abrupt changes of 50 Å or more on an otherwise nearly planar crystal surface. The images of lysozyme previously reported have been obtained with the force mode. In contrast, data collected on protein surfaces while operating in height mode generally cannot be interpreted in their raw form as easily as can those collected in force mode. The height data, however, contain more information that may be extracted with data-reduction procedures.

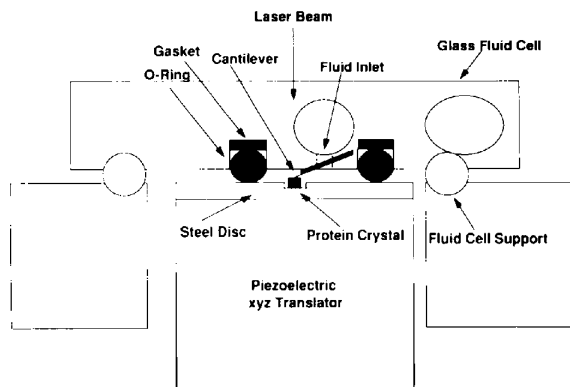


Fig. 1. AFM fluid cell used for imaging protein crystals in aqueous solution.

This paper describes the types of quantitative information that may be obtained concerning the surface of single crystals of lysozyme by analyzing data that is collected in height mode. We will first describe the data-collection procedure. Then, the data-reduction procedures employed to obtain three-dimensional images illustrating growth steps and dislocations is briefly explained. Several methods for quantitatively measuring and displaying crystal growth or dissolution are then presented. Finally, high-resolution images possessing molecular (or near molecular) resolution are presented along with model images of the possible lysozyme surfaces that would be observed with different tip shapes.

## 2. Experimental

Crystals were grown in an incubator at 295.8 K from a solution containing 40 mg ml<sup>-1</sup> hen egg-white lysozyme, 5% by weight sodium acetate and 5% by weight sodium chloride. 0.5 ml of solution was added to each well of a Linbro crystallization tray. The reservoirs were sealed with clear packaging tape, which was cut around each well for harvesting. Crystals suitable for examination were obtained within 1 d. The crystallization tray was examined at 30× magnification for selection of a crystal. The crystal to be examined was isolated with tweezers and drawn up into a 15 cm long Pasteur pipette. The solution was then deposited onto a 15 mm stainless steel disc, which was magnetically secured in the AFM on the piezo stage. To secure the protein crystal, the stainless steel AFM disc was modified by drilling an off-center 2 mm diameter hole 0.25 mm deep. Prior to transferring the solution from the Pasteur pipette this hole was filled with Apiezon M grease. The pool of mother liquor containing the

crystal was viewed under 30× magnification, and the protein crystal was gently positioned with tweezers to lie in the center of the Apiezon-filled well and then pressed into the grease, while the surface reflection of the crystal was monitored for flatness. Once the crystal was mounted, the disc was transferred to the piezo stage and viewed through the Nikon Optizoom optical microscope on a video monitor (Fig. 2). The appropriate crystal orientation was chosen; two drops of stabilizing solution that contained 5 mg lysozyme ml<sup>-1</sup>, 5% sodium acetate and 5% sodium chloride were added to the fluid cell, and it was placed atop the protein crystal. The fluid cell contained an 'o' ring which forms a seal on the steel disc to prevent evaporation. For large crystals a Teflon washer was added to the 'o' ring groove to extend the projection to form a seal. Optical images of the crystal orientation, with tip for scaling, were captured using either a video cassette recorder or a video copy processor.

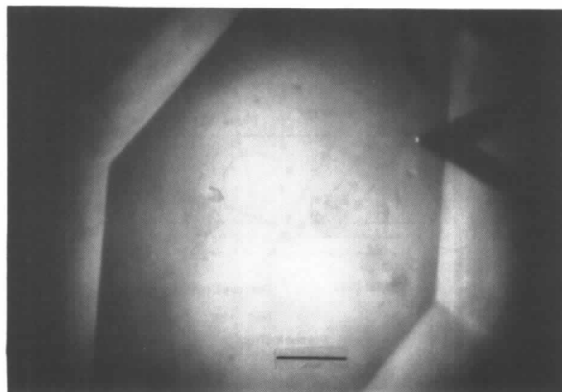


Fig. 2. The 'top view' feature of the AFM. The TV and binocular microscope permit viewing the sample and tip from above while selecting the area of the crystal to be investigated. The horizontal bar represents 100 μm.

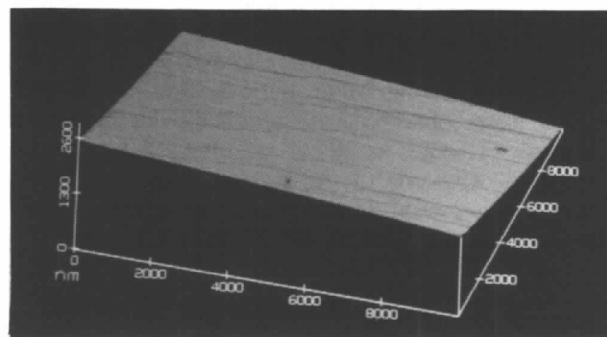


Fig. 3. An unprocessed image collected in height mode.

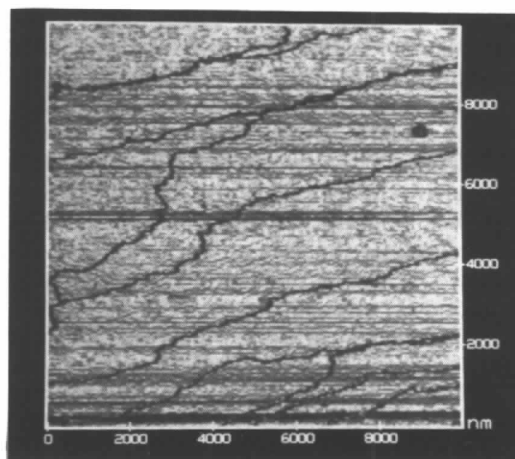


Fig. 4. The image shown in Fig. 3 after it has been leveled as described in the text. Note the horizontal stripes which are due to discontinuities between adjacent scan lines.

Using the capability of the microscope to view the crystal and cantilever tip holder from above (Fig. 2), the tip was manually positioned and lowered close to the protein crystal surface. Care was taken to level the fluid cell mount. The tip was automatically engaged and, upon engagement, the force curve was examined and set for minimal force. A low-resolution survey was made over a 3000–10000 nm square area to detect the presence of growth or dissolution steps, and then molecular resolution images were collected over smaller ( $30 \times 30$  nm) areas of interest. Once reproducible data were obtained, the AFM was transferred to an isolation

platform suspended from four bungee cords, extending approximately 1 m from the ceiling. This arrangement offered acoustical isolation down to a few Hertz. Additional acoustical isolation was provided by adding a Barium-loaded vinyl membrane to the inside of the aluminum wind cap.

### 3. Data reduction

Fig. 3 displays an unprocessed image of the (110) face of lysozyme. We wished to reorient the image such that the  $z$  direction was normal to the planar surfaces. This was accomplished by rotating the

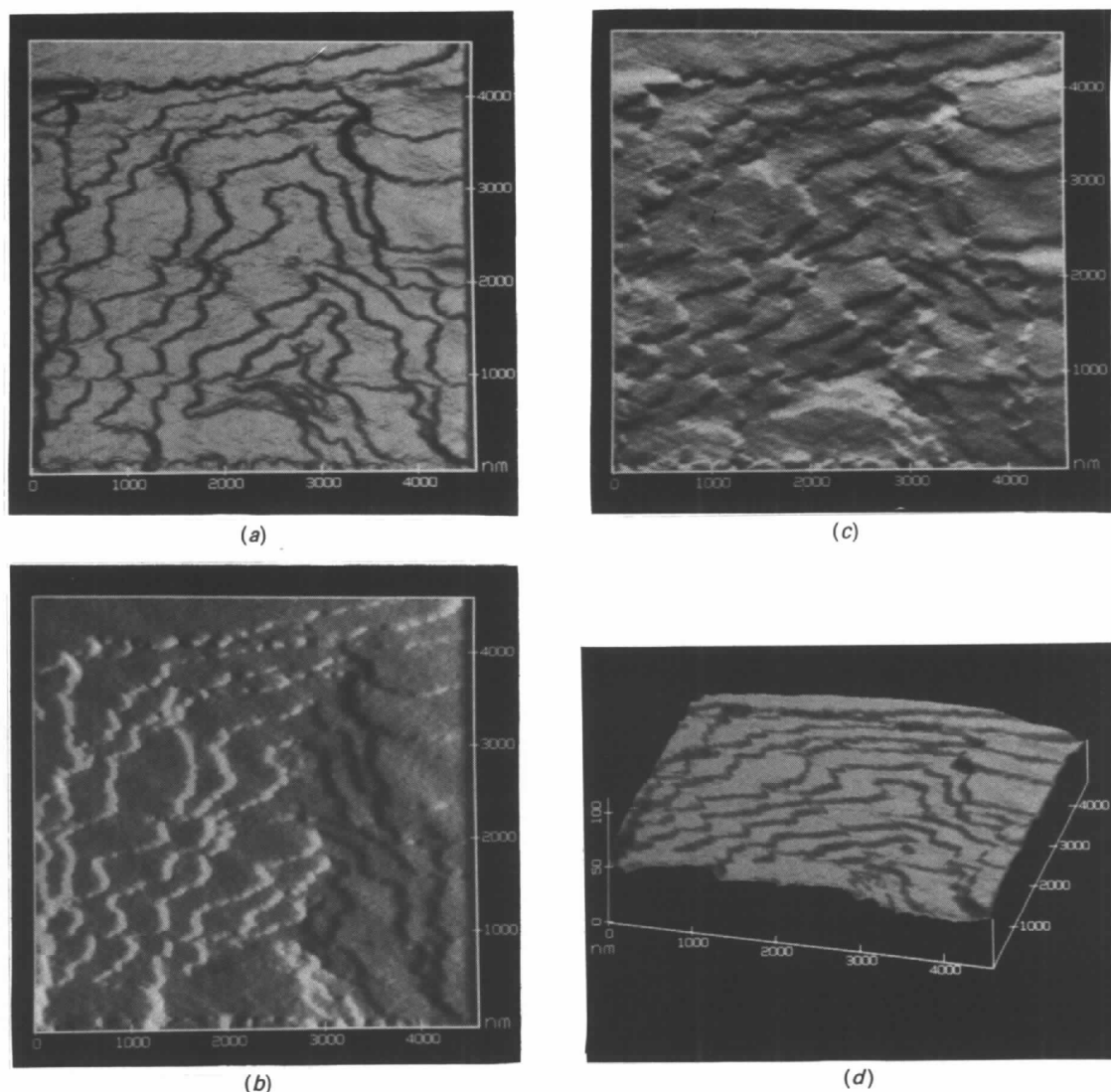


Fig. 5. (a) Top view of a pit in a (110) surface after the image has been both leveled and had the scan line discontinuities removed by a procedure described in the text. (b) A plot of the scan line slopes,  $dz/dx$ , for the image shown in (a). This corresponds to the image that would have been obtained with the microscope operating in force mode. (c) A plot of the slopes perpendicular to the scan lines,  $dz/dy$ , for the image shown in (a). Note the information complementary to (b). (d) Surface plot of the image shown in (a).

image such that the slopes of the planar surfaces were near zero in the  $x$  and  $y$  directions. The slopes at the growth steps, which have large absolute values, were excluded on this basis from the leveling calculation. Fig. 4 displays the leveled image. The individual scan lines which comprise the image are evident in Fig. 4. These artifacts are the result of the translations of the  $x$  piezoelectric crystal not being quite reproducible for the same voltage on successive scan lines. The voltages corresponding to a specific  $z$  value drift. This displacement is not constant for all

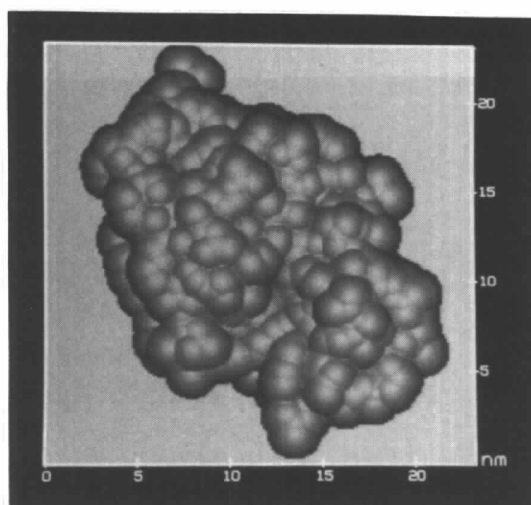


Fig. 6. Plot of the theoretical surface for a single lysozyme molecule expanded approximately fivefold in linear dimension.

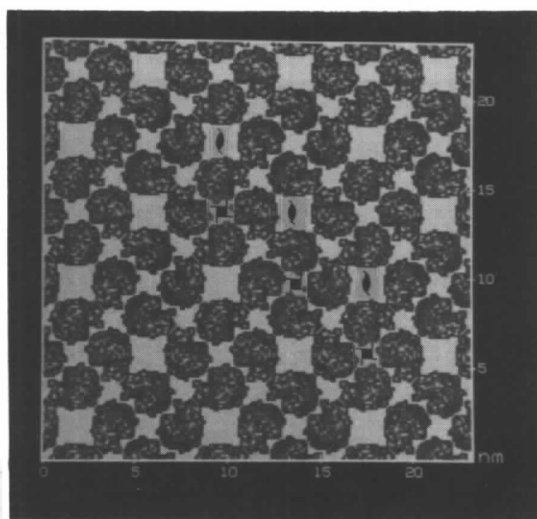


Fig. 7. The structure of tetragonal lysozyme viewed along the  $c$  direction. The two unique (110) cleavage planes possible contain either fourfold screw axes (referred to as face F1 in the text) or twofold screw axes (referred to as face F2 in the text).

data points in adjacent scan lines. To correct for this, we have devised a procedure that 'warps' adjacent scan lines attempting to eliminate these discontinuities in  $z$ , while restraining the slopes within scan lines to remain near their experimentally measured values (Konnert, 1994). The corrected surface values for Fig. 4 will be discussed below and are illustrated in Fig. 10.

The processed image for a region containing a pit in the surface of a face is illustrated in Fig. 5(a). Fig. 5(b) is a plot of the slope in the  $x$  direction of every point on the surface displayed in Fig. 5(a). Since the  $x$  direction is the direction in which the tip scans, this figure corresponds very closely to the image that would have been obtained directly had the microscope been operated in force mode. Indeed, this illustrates that it would be desirable for the microscope to possess an option that displays the slope of the scan lines as height data are being recorded. Our data-collection software is contained in a 'black box',

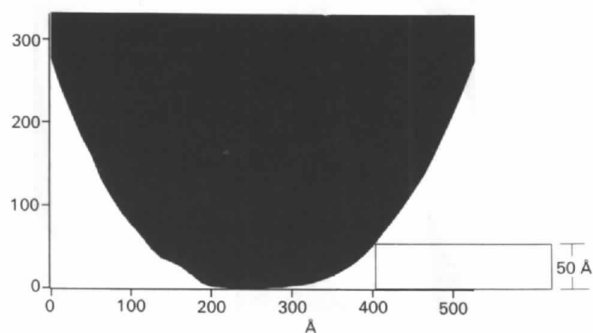


Fig. 8. Schematic depicting a tip with a radius of approximately 200 Å adjacent to a growth step of 50 Å.

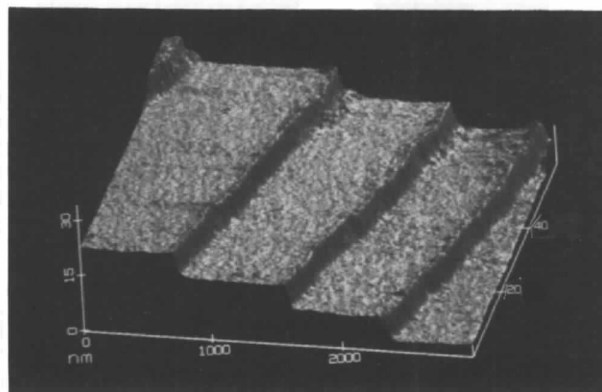


Fig. 9. Evolution of growth steps with time. The image is composed of 200 repeated scans along the same line on the (110) face. The  $y$  axis, reading away from the viewer, represents a time span of 60 s.

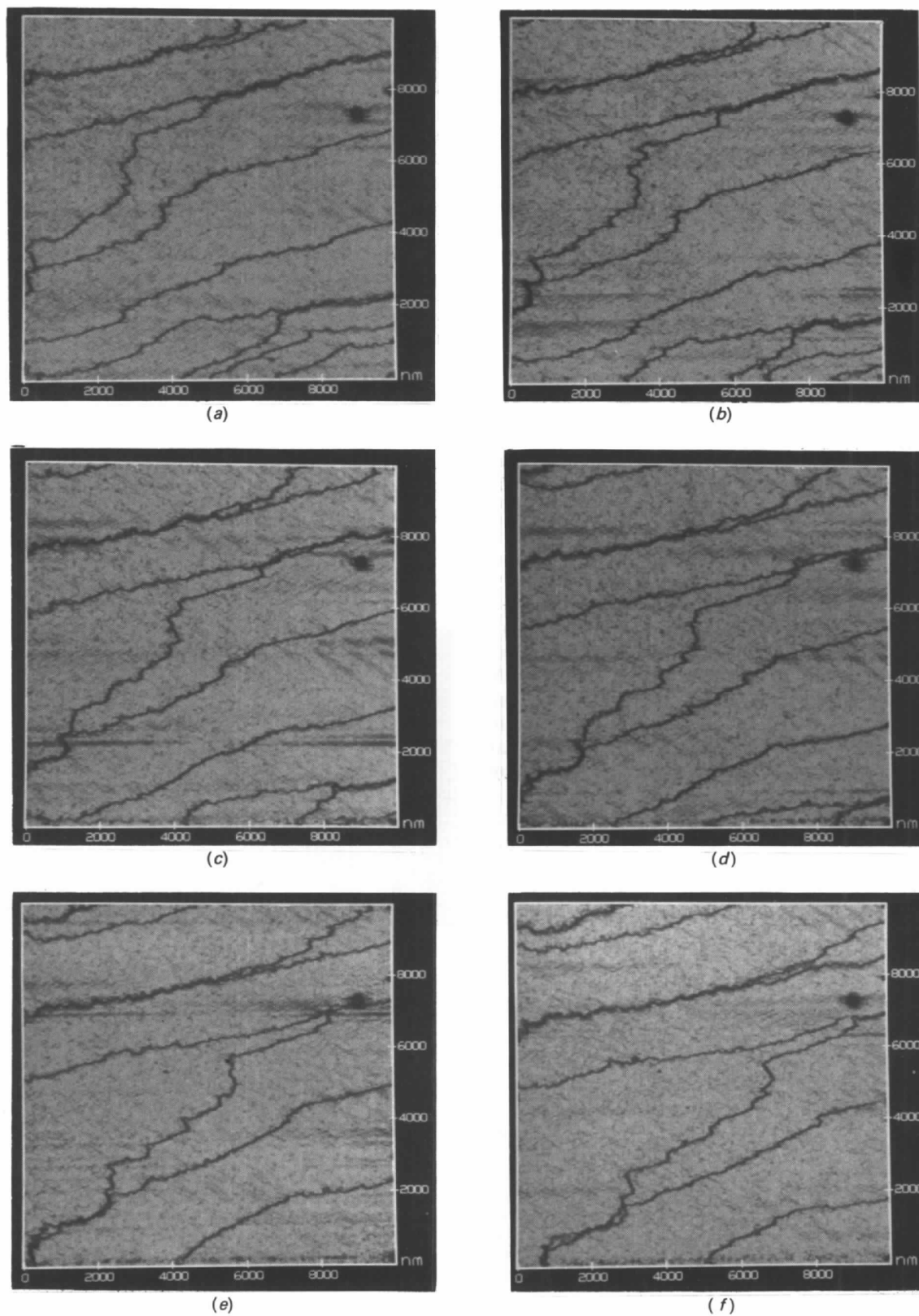


Fig. 10. (a)–(f) Six consecutive images of a (110) face collected at one minute intervals. The steps are moving from the top left towards the bottom right. The dark spot in the upper right is a hole in the surface that remains stationary during the experiment.

so we accomplished this by post-processing the data. Additionally, we plotted the slope in the  $y$  direction for every point on the surface, Fig. 5(c). This highlights details complimentary to Fig. 5(b). Fig. 5(d) is a surface plot that conveys the three-dimensional nature of these data.

The same data-reduction procedure was employed for the molecular-resolution data to be discussed below. Since we wish to relate the observed surfaces to the arrangements of the molecules within the crystal, it was useful to examine the shape and arrangement of the molecules within the crystals as determined by X-ray diffraction.

#### 4. Structure of tetragonal lysozyme crystals

To facilitate the interpretation of the images, we have written a computer program with which the theoretical surface exposed by cleaving an ideal crystal structure along an arbitrary plane may be observed. A theoretical surface is constructed by enclosing the mean atomic positions within shells of arbitrary radius. The  $z$  coordinates for this surface are then sampled on an  $xy$  grid corresponding to the one employed in AFM data collection. The theoretical surface is then placed in a file with a format such that it may then be displayed and examined with the same graphics programs used for the AFM data. Fig. 6 displays the surface of a single lysozyme molecule in this format. The program also permits the evaluation of the surface accessible for an arbitrarily shaped tip. This will be illustrated below when the high-resolution images are evaluated.

Fig. 7 displays the crystal structure of tetragonal lysozyme viewed along the  $c$  axis. The crystallographic cell dimensions are  $a = b = 37.9$  and  $c = 79.1$  Å. The positions of the screw axes are noted. All of the images examined in this paper were obtained

from (110) faces. The two unique (110) cleavage planes in the crystal structure run diagonally in Fig. 7, and are perpendicular to the plane of Fig. 7. A smooth (110) surface may be obtained by cleaving the crystal along a plane containing either the four-fold screw axes (F1 in Fig. 7) or a plane containing the twofold screw axes (F2). Analyses of the high-resolution images, to be discussed below, appear to indicate that (F2) is the predominant cleavage plane. The periodicities on the (110) face are 37.9 Å and  $2^{1/2}$  times 79.1 Å (111.86 Å). In order that the molecular outlines are clearly visible, each molecule in Fig. 7 is centered at its true value but has been reduced to 7/10 of its true linear dimensions.

Scanning electron microscope images of the prepared surfaces of lysozyme crystals (Durbin & Feher, 1990) have shown growth steps, and fine details near the edges of the steps have strongly suggested that the (110) faces grow in layers that are two molecules thick. If this is the case, the AFM should reveal steps that are 56 Å in height for a double layer. Analyses of our images indicate that the layers are predominantly, but not exclusively, two molecules thick.

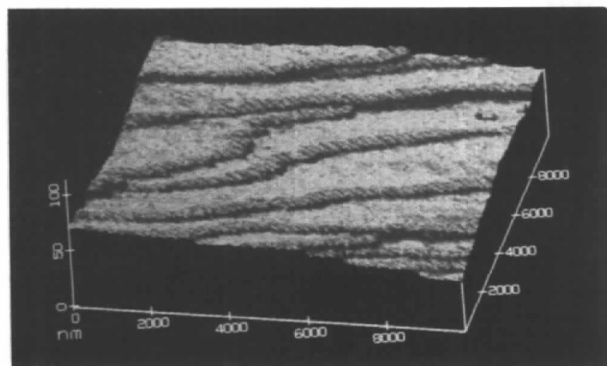
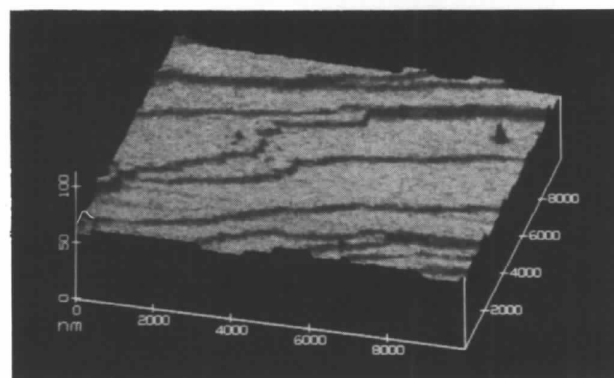
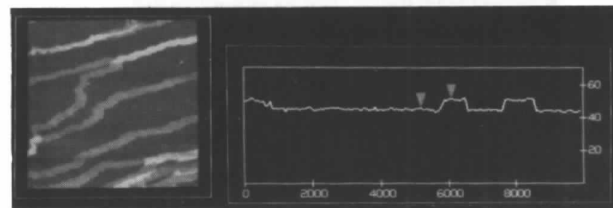


Fig. 11. Image shown in Fig. 10(b) with the furrowed regions indicating the material that has been added to the surface since the scan shown in Fig. 10(a).



(a)



(b)

Fig. 12. (a) Image in Fig. 10(a) subtracted from Fig. 10(b) showing where growth has occurred. Along the near edge one bimolecular layer has been added in some areas, and two layers in others. (b) Same as (a), but with height represented by grey scale. The predominant dark shade indicates regions of no growth. The lighter region indicates where one bimolecular layer has been added, and the lightest regions, where two layers have been added. The line graph to the right is a cross section across the top of the image. The triangular markers indicate a height of 55 Å. One bimolecular layer would correspond to a 56 Å step.

### 5. Scanning tip perturbation of crystal growth

The microfabricated silicon nitride tips (6) are advertised as having a tip radius of approximately 200 Å. Fig. 8 depicts such a tip relative to a sample step of 50 Å. Viewing such a figure suggests that a rapidly scanning tip could inflict considerable damage at the step, even if the force being exerted vertically is extremely small (about 1 nN). Possible perturbation of the growth steps was investigated by repeatedly scanning along the same line on a (110) face. Fig. 9 was obtained by disabling the  $y$  scanner. Thus, the  $y$  coordinate, receding from the observer, represents time, not distance. The illustration is composed of 200 scan lines collected in 60 s. The crystal has

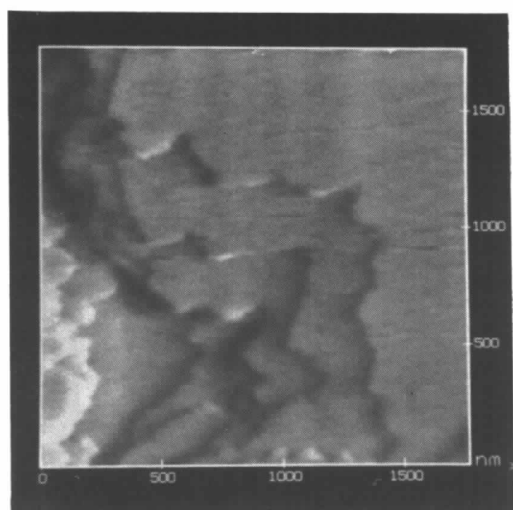
clearly continued to grow while being scanned. This image was obtained by applying the minimum force with the tip that would maintain contact with the surface.

### 6. Observation and display of crystal growth and dissolution

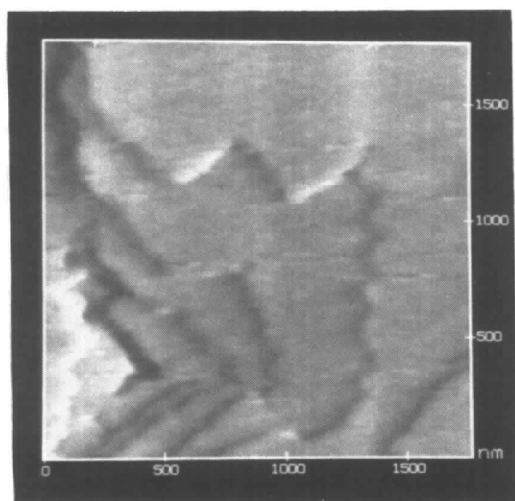
The progress of a growing face within a time span of 6 min is illustrated with the sequence of six images contained in Fig. 10. The ledges are progressing towards the lower right of the illustrations. The pit in the surface (the dark spot in the upper right) remains stationary and is overtaken by the approaching step.

Several techniques were employed to examine the progression of surface features with time. Fig. 11 combines Figs. 10(a) and 10(b). The textured regions represent the growth that has occurred between the time at which the images were captured. This growth may also be depicted by displaying Fig. 10(b) minus Fig. 10(a). This difference is displayed two different ways in Fig. 12.

Simultaneous growth and dissolution have been observed within pits on the surface. Figs. 13(a) and



(a)



(b)

Fig. 13. (a), (b) Images of a pit in a (110) surface that were collected one minute apart. Some regions have grown, whereas others have dissolved.

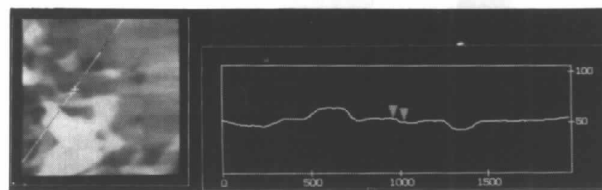


Fig. 14. The difference between images in Figs. 13(a) and 13(b). The light regions indicate where the crystal has grown, and the dark regions show where it has dissolved. The cross section, indicated by the line on the image, is shown at the right. Note that the markers indicate an area where it appears that one molecular layer (33 Å measured *versus* 28 Å for ideal) has been added.

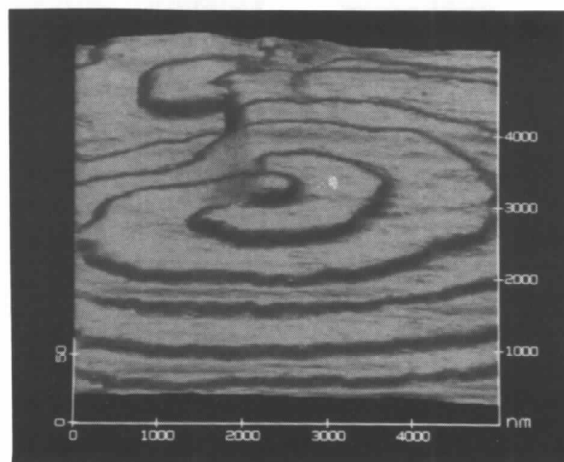


Fig. 15. Processed images of a spiral dislocation.

13(b) were collected one minute apart. The difference curve in Fig. 14 indicates regions of growth with the lightest shades and dissolution with the darkest shades.

Image of a spiral dislocation on the (110) face of lysozyme is displayed in Fig. 15. We have not yet examined the fine details contained in these images. It is interesting to note that the dislocation occurs abruptly at its apex.

### 7. Observation of molecular packing and crystallographic periodicity

Four of the high-resolution images that have been obtained of the (110) face are shown in Fig. 16. If the

surface structure is the same as bulk structure and no surface reconstruction has occurred, the surface structure(s) should be similar to one or both of the faces that were earlier referred to as F1 and F2. These two surfaces are illustrated in Fig. 17. Again, the molecules have been displayed both with their full linear dimensions and with reduced linear dimensions in order that the individual molecules may be easily discerned. Both F1 and F2 exhibit the symmetry of plane group  $p4gm$  and have translational lengths of 38 Å (vertical) and 112 Å (horizontal), which agree with the X-ray lattice spacings of  $a = b = 79.1$  and  $c = 37.9$  Å, with diagonal spacing 111.9 Å.

The high-resolution images were enhanced using the data-reduction procedures described above. The pro-

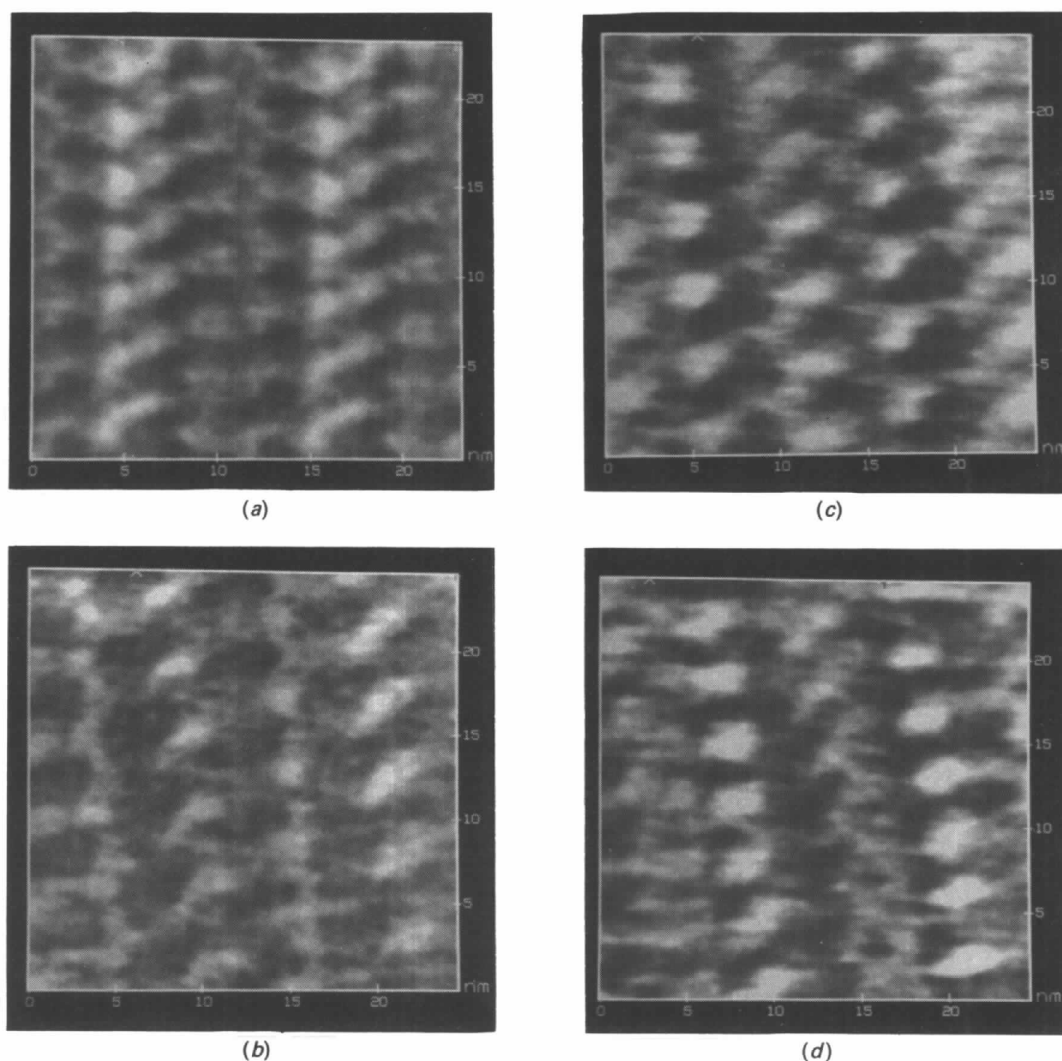


Fig. 16. (a)–(d) Processed images showing high-resolution details on the (110) surfaces. The crystallographic periodicities of 112 Å horizontally and 38 Å vertically are apparent in each image. (a) may resolve individual molecules (see Fig. 19b).

gress of each step in these procedures is illustrated in Figs. 18(a)–18(d) for a data set similar to, but different from, those depicted in Fig. 16. Fig. 18(a) is the raw data; Fig. 18(b) is the flattened data; Fig.

18(c) has had the adjacent scan lines warped to eliminate discontinuities in  $z$ ; Fig. 18(d) has been translationally averaged in the direction of the 38 Å repeat. This last type of image enhancement was

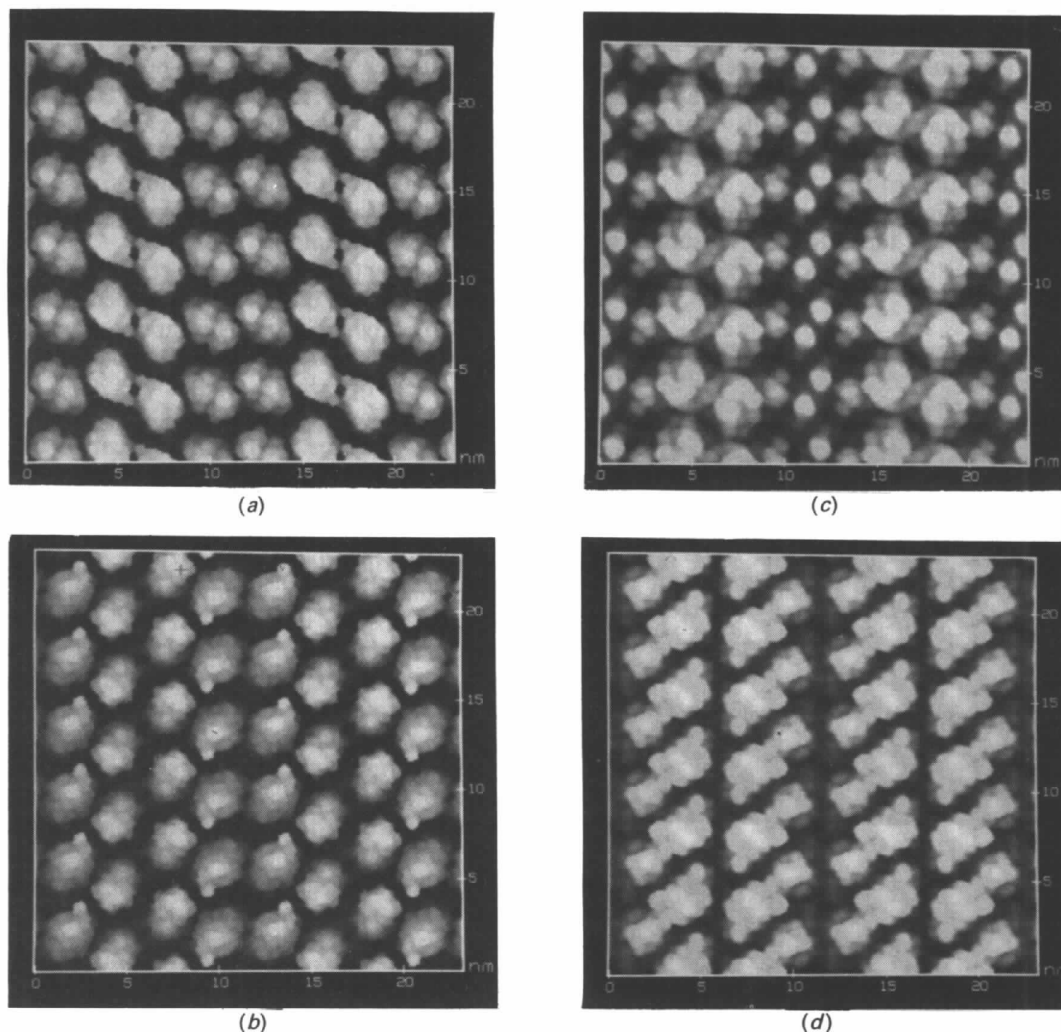


Fig. 17. (a) The F1 (110) face with the molecules drawn at 0.7 of their linear dimensions. (b) Same as (a) with full linear dimensions. (c) The F2 (110) face with the molecules drawn at 0.7 of their linear dimensions. (d) Same as (c) with full linear dimensions.

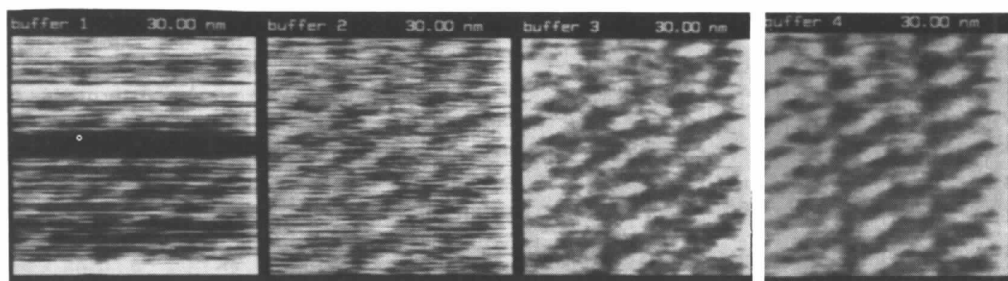


Fig. 18. (a) An unprocessed high-resolution image. (b) Image after (a) has been flattened. (c) Image after (b) has had scan-line discontinuities removed. (d) Image after vertical translation averaging of (c).

applied only to the high-resolution data. A periodicity of near  $38 \text{ \AA}$  is observed approximately along the vertical direction of Fig. 18(c). Each point in Fig. 18(d) is the average of three (or two) points in Fig. 18(c). These points are  $(x - dx, y - dy)$ ,  $(x, y)$  and  $(x + dx, y + dy)$  where  $dx$  and  $dy$  define the direction of the approximate  $38 \text{ \AA}$  periodicity. This type of averaging is preferable to selecting Fourier components when either a limited number of repeats are present in the image or the periodicity is only approximate due to instrumental errors. Details that have the short-range periodicity defined by  $dx$  and  $dy$  will reinforce one another in Fig. 18(d).

The most striking common features of the high-resolution images are the observed crystallographic

periodicities of  $112 \text{ \AA}$  horizontally and  $38 \text{ \AA}$  vertically. Each such two-dimensional unit cell would expose the surface of four molecules, if the surface structure is similar to the internal structure. Fig. 16(a) may resolve individual molecules (see Fig. 19b to be discussed below). Another feature that recurs is the nearly centered periodic array of minima. The periodicities, of course, occur in both of the possible ideal surfaces, F1 and F2. The centered array of minima, however, occurs only in F2. This will be seen readily when the tip-accessible surfaces are discussed below. The images in Fig. 16 differ in their fine detail. Two of the possible reasons for the observed variations are different surface structures and different tip shapes.

The facility to model the effects of tip shape on the images observed has been developed. The surfaces traced by tips of various shapes approaching the surfaces illustrated in Fig. 17 has been investigated. A spherical tip with a radius of  $200 \text{ \AA}$  yields no information on the molecular packing. The 'tip-accessible' surfaces for F2 and F1 with a tip  $40 \text{ \AA}$  in radius are illustrated in Figs. 19(a) and 19(b). The surface associated with F2, Fig. 19(a), contains a centered array of minima similar to those observed in the experimental patterns (Figs. 16a-d and Fig. 18). Perhaps more importantly, the maxima in Fig. 16(a) agree quite closely with the positions of the individual molecules in Fig. 19(a). A comparison of Fig. 17(c) with Fig. 19(a) shows that the individual molecules could be resolved with a spherical tip possessing a radius of  $40 \text{ \AA}$ . The central vertical band in the experimental image shown in Fig. 16(a) may correspond to the central vertical band of somewhat deeper molecules displayed in the theoretical surface of Fig. 19(a). Such a centered array is not observed in Fig. 19(b). Our analysis indicates that the differences in the maximum and minimum  $z$  values are about  $5 \text{ \AA}$  for Fig. 19(a) as compared to  $2 \text{ \AA}$  for the experimentally determined images. Thus, the theoretically calculated 'tip-accessible' surface has relief similar in value to that of the experimentally obtained surfaces.

## 8. Concluding remarks

This survey of some of the types of quantitative information about surfaces of lysozyme crystals that may be obtained with an AFM indicates that it may be a very useful tool in studying the mechanisms of crystal growth. In favorable instances, the tip perturbs the surface to such a sufficiently small extent that there appears to be a real possibility of observing not only the location of individual molecules, but also their shapes. At one step lower in resolution, it will be interesting to investigate the fine details of defects such as screw dislocations. Do the

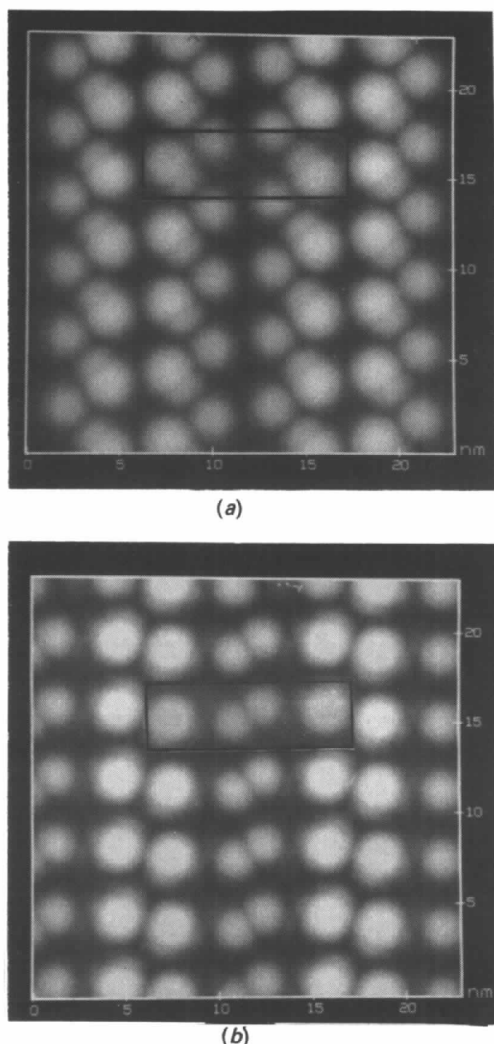


Fig. 19. (a) Theoretical 'tip accessible' surface of an F2 layer employing a spherical tip of  $40 \text{ \AA}$  radius. (b) Theoretical 'tip accessible' surface of an F1 layer employing a spherical tip of  $40 \text{ \AA}$  radius

dislocations occur continuously as one progresses around the screw? What is the nature of growth and dissolution within pits where many crystal surfaces are exposed? Much interesting work remains to be carried out in applying these techniques.

This research was supported by the Office of Naval Research and NASA Grant H-07973D.

#### References

- Digital Instruments (1990). *Nanoscope II Manual*. Version 5. Digital Instruments, Santa Barbara, CA 93103, USA.
- DURBIN, S. D. (1993). *Conference on Protein Crystal Growth in Microgravity*, Panama City, Florida.
- DURBIN, S. D. & CARLSON, W. E. (1992). *J. Cryst. Growth*, **122**, 71-79.
- DURBIN, S. D. & FEHER, G. (1990). *J. Mol. Biol.* **212**, 763-774.
- KONNERT, J. H. (1994). In preparation.